COMMUNICATIONS CHEMISTRY

ARTICLE

https://doi.org/10.1038/s42004-019-0142-3 OPEN

Photochemical nitrogenation of alkanes and arenes by a strongly luminescent osmium(VI) nitrido complex

Jing Xiang[1,2], Xin-Xin Jin[1], Qian-Qian Su[1], Shun-Cheung Cheng[2], Chi-Chiu Ko[2], Wai-Lun Man[3], Minying Xue[4], Liangliang Wu[5], Chi-Ming Che[4] & Tai-Chu Lau[2]

The search for a highly active nitrido complex that can transfer its nitrogen atom to inert organic molecules remains a challenge to chemists. In this regard, the use of solar energy to generate a reactive nitrido species is an appealing strategy to solve this problem. Here we report the design of a strongly luminescent osmium(VI) nitrido compound, $[Os^{VI}(N)(\mathbf{NO_2\text{-}L})(CN)_3]^-$ (**NO_2-OsN**) with emission quantum yield (Φ) and life time (τ) of 3.0% and 0.48 μs, respectively in dichloromethane solution. Upon irradiation with visible light, this complex readily activates the aliphatic C-H bonds of various hydrocarbons, including alkanes. The excited state of **NO_2-OsN** can undergo ring-nitrogenation of arenes, including benzene. Photophysical and computational studies suggest that the excited state of **NO_2-OsN** arises from O^N ligand to Os ≡ N charge transfer transitions, and as a result it possesses [Os = N•] nitridyl character and is highly electrophilic.

[1] College of Chemistry and Environmental Engineering, Yangtze University, Jingzhou 434020 Hubei, People's Republic of China. [2] Department of Chemistry, City University of Hong Kong, Tat Chee Avenue, Kowloon Tong, Hong Kong 999077, People's Republic of China. [3] Department of Chemistry, Hong Kong Baptist University, Kowloon Tong, Hong Kong 999077, People's Republic of China. [4] Department of Chemistry and State Key Laboratory of Synthetic Chemistry, The University of Hong Kong, Pokfulam Road, Pokfulam, Hong Kong 999077, People's Republic of China. [5] Department of Chemistry, Southern University of Science and Technology, Shenzhen 518055 Guangdong, People's Republic of China. These authors jointly supervised: Jing Xiang, Chi-Chiu Ko, Chi-Ming Che, Tai-Chu Lau. Correspondence and requests for materials should be addressed to T.-C.L. (email: bhtclau@cityu.edu.hk)

Transition metal nitrido (M≡N) complexes are key intermediates in N_2 fixation; they are also potentially useful reagents for the nitrogenation of various organic substrates[1–3]. Although a variety of transition metal nitrido complexes are known, few have oxidizing ability that are comparable to metal-oxo species, such as $Fe^{IV}(O)P^{+\bullet}$ in cytochrome P_{450} enzymes[4,5]. Pioneering work by Meyer and Huynh[6] has shown that $[Os^{VI}(terpy)(N)Cl_2]^+$ (terpy=2,2′:6′,2″-terpyridine) and related complexes are highly electrophilic/oxidizing; they react with a variety of organic substrates resulting in the formation of novel osmium complexes in lower oxidation states. However, these complexes do not undergo C–H bond activation, especially for substrates with unactivated C–H bonds, such as alkanes. Previous studies have demonstrated that the ruthenium(VI) nitrido complexes bearing salen-type ligands are highly electrophilic[7]; in particular, the complex [Ru(N)(salchda)(MeOH)]$^+$ (salchda=*N*,*N*′-bis(salicylidene)-*o*-cyclohexyldiamine dianion) is the only well-defined nitrido complex that is able to activate the C–H bonds of alkanes in the presence of pyridine[8]. A number of azido complexes, including $Ru_2(D(3,5\text{-}Cl_2)PhF)_4N_3$ (D(3,5-Cl_2)PhF=*N*,*N*′-bis(3,5-dichlorophenyl) formamidinate)[9,10], (^{iPr}BPDI)CoN_3 (^{iPr}BPDI=2,6-(2,6-^{i}Pr$_2$-C_6H_3=CPh)$_2C_5H_3N$)[11], $[(^3PDI_2)Co_2(\mu\text{-}N_3)(PMe_3)_2][OTf]_3$ (PDI=2,6-pyridyldiimine)[12], $Ni(Et_3P)_2(N_3)_2$[13] and $(C_5Me_5)_2U[N(SiMe_3)_2](N_3)$[14] can also undergo inter- or intramolecular C–H bond activation of alkanes and arenes via in situ generation of putative nitrido intermediates by thermolysis or photolysis.

Apart from the above systems, the use of solar energy to generate highly reactive nitrido complex in the excited state for the nitrogenation of organic substrates is an appealing approach. A number of d^2 nitrido complexes, such as those of Re^V and Os^{VI}, have long-lived emissive excited states[15–21]; the emissions of these complexes were shown to originate mainly from metal-centered ligand field $^3[(d_{xy})^1(d_{\pi^*})^1]$ excited states. Although some of these complexes are strong one-electron oxidants in their excited states, nitrogen atom transfer reactions of these complexes, especially towards inert organic substrates, have not been demonstrated.

Recently, we reported the synthesis of an osmium(VI) nitrido complex $[Os^{VI}(N)(\mathbf{L})(CN)_3]^-$ (**OsN**, **HL**=2-(2-hydroxyphenyl) benzoxazole) via the oxidation of an osmium(III) guanidine precursor $[Os(\mathbf{L})\{N(H)C(NH_2)_2\}(CN)_3]^-$ (**OsG**)[22–24]. In this work, we have synthesized a nitro derivative of **OsN** $[Os^{VI}(N)(\mathbf{NO_2\text{-}L})(CN)_3]^-$ (**NO_2-OsN**, **NO_2-HL** = 2-(2-hydroxy-4-nitrophenyl)benzoxazole via a similar procedure. The photophysical and photochemical properties of the two complexes have been investigated. **OsN** is very weakly emissive in both the solid state and fluid solution. In contrast, **NO_2-OsN** is highly luminescent in both solid state and fluid solutions. More importantly, to the best of our knowledge, under visible-light excitation **NO_2-OsN** becomes the most oxidizing/electrophilic nitrido species reported. It readily undergoes aliphatic C–H bond activation of hydrocarbons and ring-nitrogenation of arenes.

Results

Synthesis and characterization of NO_2-OsN. The synthesis of **NO_2-OsN** is summarized in Fig. 1.

NO_2-OsN was isolated as light yellow PPh_4^+ salt in 35% yield. Consistent with its $(d_{xy})^2$ ground state electronic configuration, this compound is diamagnetic (μ_{eff} ~0 μ_B), as evidenced by the sharp resonances in the normal range in the ^{1}H nuclear magnetic resonance (NMR) spectrum (Supplementary Fig. 1). The electrospray ionization/mass spectrometry (ESI/MS) of **NO_2-OsN** in MeOH (−ve mode) shows the parent anion $[M]^-$ at *m/z* 539, which is shifted to *m/z* 540 in the ^{15}N-labeled complex **NO_2-Os^{15}N** (Supplementary Fig. 2). In the infrared (IR) spectrum, the ν(Os≡N) stretch is found at 1074 cm^{-1}, which is shifted to 1046 cm^{-1} upon ^{15}N labeling.

The molecular structure of **NO_2-OsN** has been determined by X-ray crystallography (Fig. 2a, Supplementary Table 1 and Supplementary Data 1). Similar to **OsN**, the three cyano ligands are in *meridional* configuration and the nitride is *trans* to the phenoxy oxygen. The Os-N (nitrido) bond lengths of both complexes are similar (1.655(3) Å for **NO_2-OsN**; 1.653(2) Å for **OsN**) and are within the range for Os≡N[25].

Photophysical properties of OsN and NO_2-OsN. The two Os(VI) nitrido complexes show intense ligand-centered $\pi\rightarrow\pi^*$ transitions of the bidentate O^N ligand (**L**/**NO_2-L**) at 230–310 nm with molar extinction coefficients (ε) of the order of 10^4 dm^3 mol^{-1} cm^{-1} (Fig. 3a). For **OsN**, there is a moderately intense broad absorption band at 357 nm with molar absorptivity (ε) ~1.2×10^4 dm^3 mol^{-1} cm^{-1} and a shoulder at 378 nm tailing down to about 500 nm. In **NO_2-OsN**, the corresponding absorption band is more intense (~3.2×10^4 dm^3 mol^{-1} cm^{-1}) and is slightly blue-shifted with λ_{max} at 365 nm. The lowest-energy absorption band in the two complexes is tentatively assigned to O^N ligand to Os≡N charge transfer (LML′CT) transitions, probably mixed with metal-centered *d*–*d* transitions $[(d_{xy})^2\rightarrow(d_{xy})^1(d_{\pi}^*)^1]$.

The LML′CT assignment is further supported by resonance Raman (RR) spectroscopic study of **NO_2-OsN** (Fig. 3c), which shows enhancements of Raman signals corresponding to the Os≡N stretching mode (assigned based on the normal Raman spectra of the unlabeled and ^{15}N-labeled complexes) and C=C, C=N, NO_2 stretches of the bidentate N^O ligand upon 355 nm excitation. This is indicative of the involvement of both the bidentate N^O ligand and Os≡N in the electronic transition of the lowest-energy absorption band and is consistent with LML′CT [π(N^O)→$d\pi^*$(Os≡N)] character. This is further supported by the results of the density functional theory (DFT)/time-dependent DFT (TDDFT) calculations.

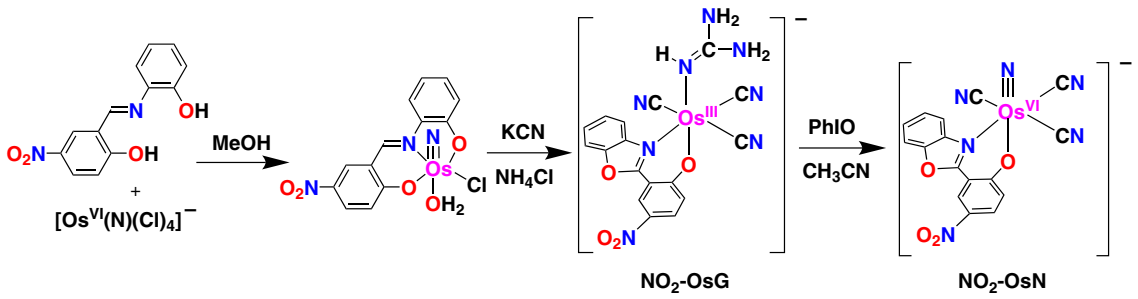

Fig. 1 Synthetic route for **NO_2-OsN**. The synthesis of **NO_2-OsG** is similar to the previous reported method for **OsG** and iodosobenzene (PhIO) is used as the oxidant

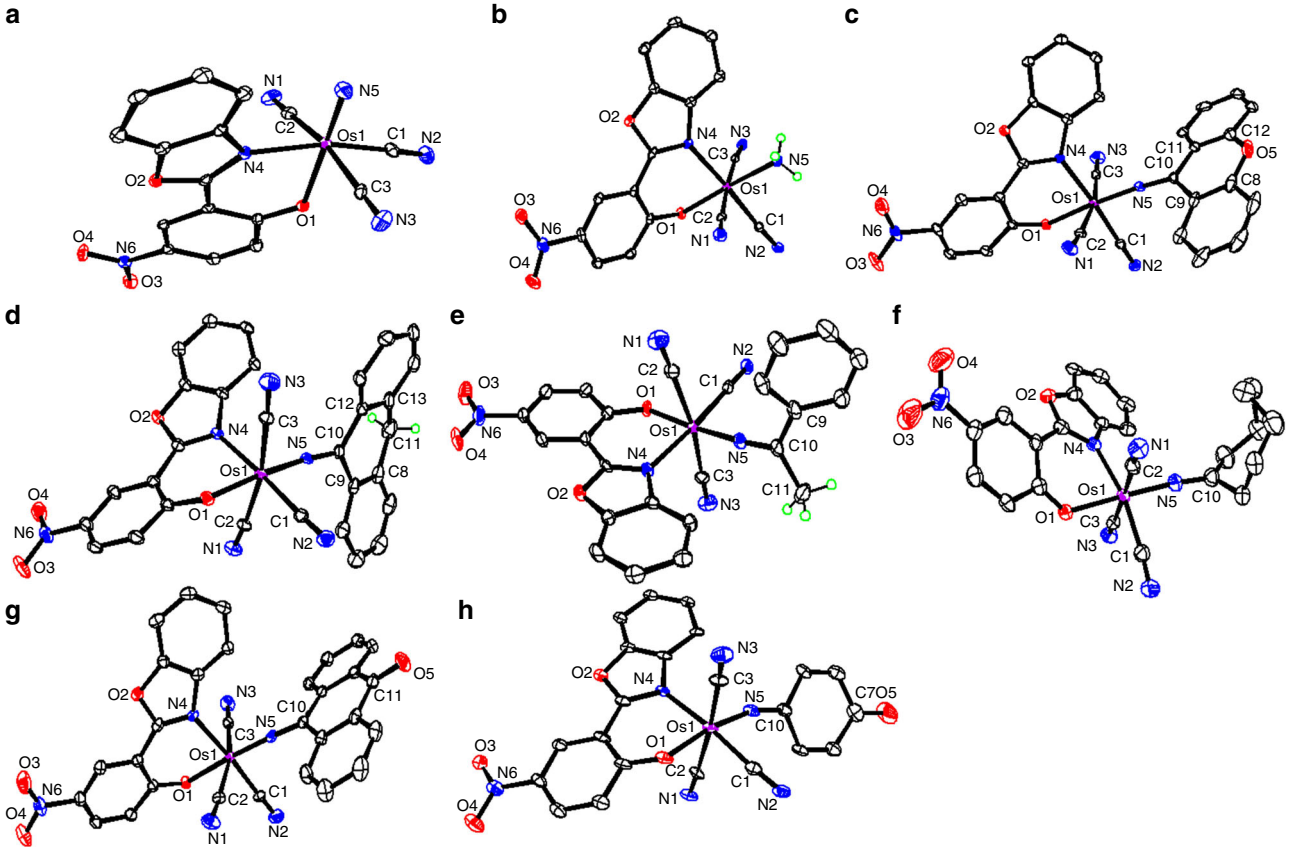

Fig. 2 Crystal characterization. The ORTEP (Oak Ridge Thermal Ellipsoid Plot) drawing of the anionic structures of **NO_2-OsN** (**a**), **1** (**b**), **2** (**c**), **3** (**d**), **4** (**e**), **5** (**f**), **7b** (**g**) and **8** (**h**)

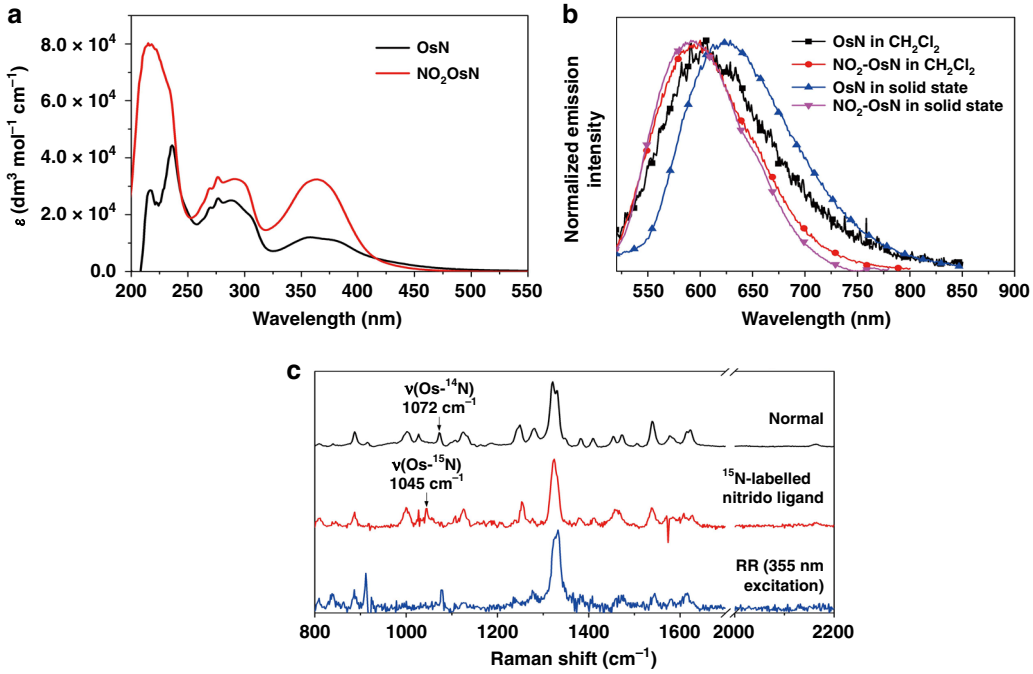

Fig. 3 Spectroscopic characterizations for **OsN** and **NO_2-OsN**. **a** Ultraviolet/visible (UV/Vis) spectra of **OsN** and **NO_2-OsN** in CH_2Cl_2 solution. **b** Emission spectra of **OsN** and **NO_2-OsN** in CH_2Cl_2 solution and in solid state at 298 K ($\lambda_{ex} = 355$ nm). **c** Normal Raman ($\lambda_{ex} = 785$ nm) and resonance Raman spectra ($\lambda_{ex} = 355$ nm) of **NO_2-OsN** in acetonitrile solution

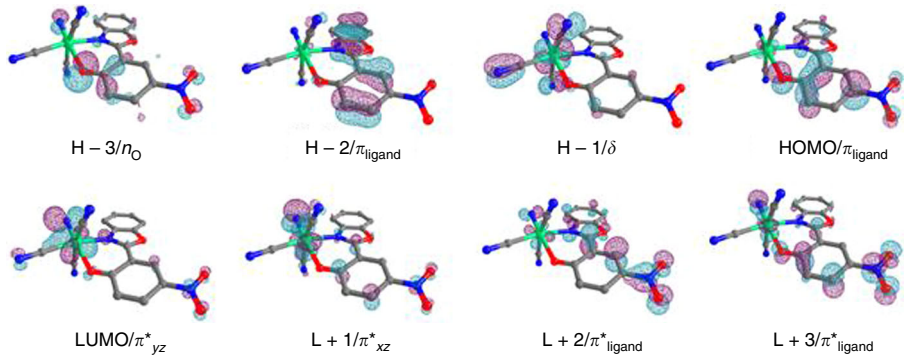

Fig. 4 Density functional theory (DFT)/time-dependent DFT (TDDFT) calculations for **NO_2-OsN**. Frontier molecular orbitals (MOs) of **NO_2-OsN** at the optimized S_0 geometries

DFT/TDDFT calculations have been performed on the osmium nitrido complexes. The frontier molecular orbital (MO) diagrams of **OsN** and **NO_2-OsN** are shown in Supplementary Figs. 3–4 and Fig. 4, respectively, and the Cartesian coordinates for optimized geometries have been summarized in Supplementary Tables 2–3. The highest occupied molecular orbital (HOMO) of both complexes are predominantly localized on the bidentate O^N ligand. The closely lying lowest unoccupied molecular orbital (LUMO) and LUMO+1 are comprised of the antibonding orbitals of Os(d_{yz})≡N^{3-}(p_y) (π^*_{yz}) and Os(d_{xz})≡N^{3-}(p_x)(π^*_{xz}), respectively. A brief summary of the 10 lowest vertical transitions is shown in Supplementary Table 4; the corresponding simulated ultraviolet (UV) spectra (Supplementary Fig. 5) computed by TDDFT calculations are in good agreement with the experimental absorption spectra of these complexes. The S_1/S_2 states for the two complexes are predominantly derived from the HOMO→LUMO/LUMO+1 transitions and therefore can be considered as LML′CT states. For S_3/S_4 states, they are derived from HOMO−1 [d_{xy}(Os)]→LUMO/LUMO+1, which can be considered as metal-centered ligand field dd states. By introducing the strong electron-withdrawing −NO_2 group, the energy level of the S_1–S_4 states are increased. Such trend is consistent with the absorption data. Since both the geometry optimizations and TDDFT calculations were performed in the gas phase, we have also simulated the absorption of **OsN** using the linear response polarizable continuum model with dichloromethane matrix to examine the effect of the solvent. As shown in Supplementary Fig. 6, the simulated spectra did not show obvious improvement.

Despite close resemblance of these two complexes, they exhibit very different emission properties (Fig. 3b). In the solid state, **OsN** exhibits a weak orange emission at 611 nm ($\Phi < 0.1\%$, $\tau =$ 0.14 μs), while **NO_2-OsN** exhibits a much stronger and longer-lived emission at 591 nm ($\Phi = 11.7\%$, $\tau = 1.90$ μs). With sub-microsecond lifetimes, these emissions are attributed to phosphorescence derived from LML′CT excited state. The blue-shifted emission observed in **NO_2-OsN** is in agreement with its LML′CT character, due to the stabilization of the π orbitals of **NO_2-L** by the strong electron-withdrawing and π-conjugating NO_2 group. In CH_2Cl_2 solution, **OsN** shows a very weak emission at 620 nm ($\Phi < 0.001\%$), while **NO_2-OsN** also displays a much strong emission at 594 nm ($\Phi = 3.0\%$, $\tau = 0.48$ μs). The enhanced phosphorescence properties of **NO_2-OsN** over that of **OsN** is possibly due to the strong electron-withdrawing effect of the –NO_2 group that could effectively stabilize the d_π(Os) orbitals and raise the energy of the ligand field excited state. In 77 K EtOH-MeOH (4:1, v/v) glassy medium, the emissions of **OsN** and **NO_2-OsN** remain structureless with maxima at 594 nm ($\tau = 1.38$ μs) and 577 nm ($\tau = 5.90$ μs), respectively (Supplementary Fig. 7 and Table 5), which are blue-shifted relative to those in CH_2Cl_2 solution. This is due to the rigidochromic effect in the low-temperature glassy medium, typically observed in phosphorescence of a charge transfer state.

Nanosecond transient absorption spectroscopy was carried out to provide insights into their emissive excited states. As shown in Supplementary Fig. 8, **OsN** exhibits no absorption features after 355 nm nanosecond laser excitation, while **NO_2-OsN** shows two absorption features at ca. 300–340 nm and 400–550 nm, with strong ground state bleaching at 340–400 nm in the transient absorption difference spectra. The observation of transient absorption feature in the visible region for **NO_2-OsN** is suggestive of the radical character involving the conjugated ligands in its emissive excited state, which is supportive of the LML′CT excited state origin.

Cyclic voltammetry of OsN and NO_2-OsN. The redox properties of these two complexes were studied by cyclic voltammetry (CV). The CV of **OsN** shows an irreversible oxidation wave at $E_{pa} =$ 1.44 V and an irreversible reduction wave at $E_{pa} = -1.17$ V vs. Saturated Calomel Electrode (SCE), which are tentatively assigned as the metal-centered $Os^{VII/VI}$ and $Os^{VI/V}$ process, respectively (Supplementary Fig. 9). Similar irreversible oxidation and reduction waves are also found for **NO_2-OsN** at $E_{pa} = 1.88$ V and −0.99 V, respectively. From the estimated E_{0-0} emission (**OsN** 2.05 eV, **NO_2-OsN** 2.15 eV) and electrochemical data (E_{pc}: **OsN** −0.93 V, **NO_2-OsN** −0.75 V vs. Normal Hydrogen Electrode (NHE)), the excited state redox potentials are estimated to be 1.13 and 1.40 V for **OsN** and **NO_2-OsN**, respectively (Supplementary Note 1)[15]. In order to support these assignments, further calculations have been conducted regarding the redox properties of the **OsN** and **NO_2-OsN**. As shown in Supplementary Table 6, the DFT-calculated redox potentials match quite well with the experimentally determined values. The spin density calculations (Supplementary Fig. 10) on the redox species reveal that the reduction of the complexes is Os≡N based and leads to a weakened triple bond (1.65 Å → 1.75 Å), whereas one-electron oxidation largely retains the Os≡N bond with the generation of ligand-centered radical.

Photostabilty of NO_2-OsN and OsN. Highly electrophilic nitrido complexes readily undergo coupling of the nitrido ligands to generate N_2[7,8]. However, both **NO_2-OsN** and **OsN** are stable upon irradiation with blue light ($\lambda > 460$ nm) for 24 h at room temperature in CH_2Cl_2 solution, as monitored by their absorption and luminescence spectra. This indicates that the excited states of

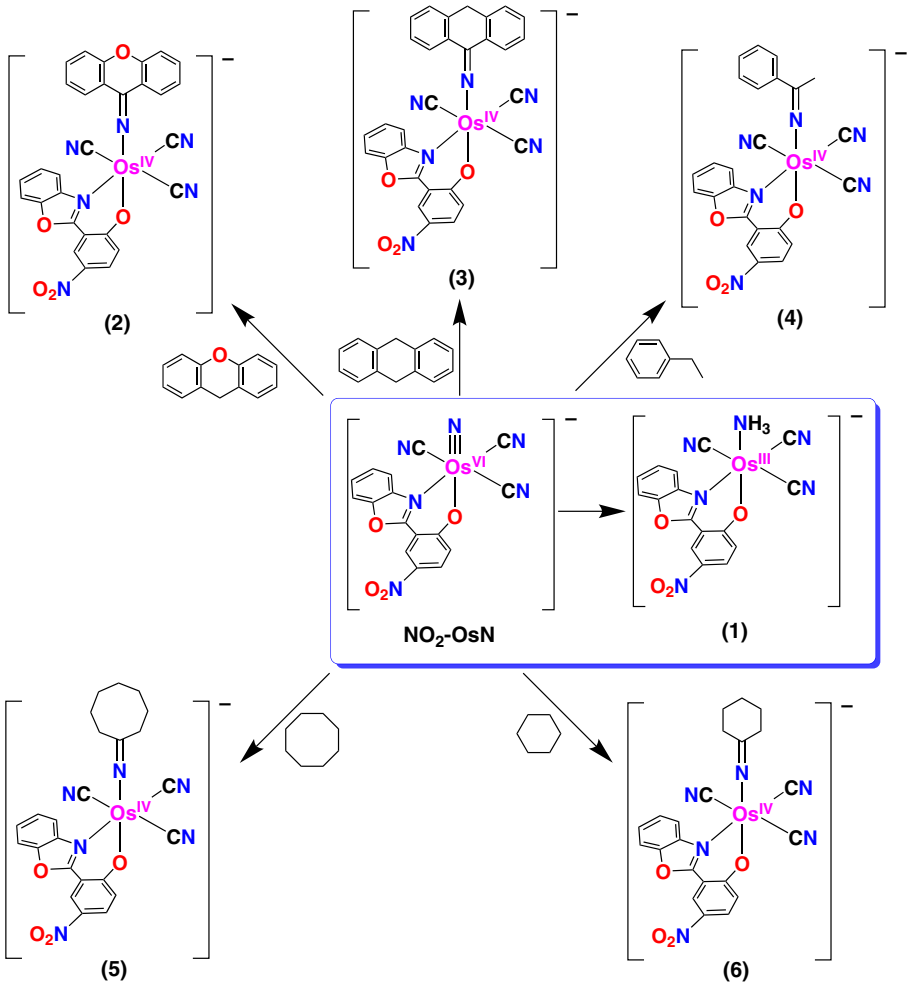

Fig. 5 Reaction of **NO_2-OsN** with various hydrocarbons. Upon visible-light irradiation of **NO_2-OsN** with hydrocarbons, the osmium(III) ammine complex **1** and osmium(IV) iminato complexes **2–6** are formed

these complexes are stable with respect to nitrido coupling or other decomposition reactions.

C-H bond activation by the excited state of NO_2-OsN (NO_2-OsN*). In accordance with the LML′CT character of its emission, **NO_2-OsN*** should possess [Os=N•] nitridyl character[26,27], which would make it highly electrophilic.

NO_2-OsN* is found to be a powerful electrophile/oxidant; it reacts readily with hydrocarbons with a wide range of C–H bond dissociation energies (BDE). The hydrocarbons investigated include xanthene (**XAN**, BDE = 75.5 kcal mol^{-1}), 1,10-dihydroanthracene (**DHA**, 78.0 kcal mol^{-1}), ethylbenzene (**EB**, 85.4 kcal mol^{-1}), cyclooctane (*c*-**OCT**, 93.6 kcal mol^{-1}) and cyclohexane (*c*-**HEX**, 95.4 kcal mol^{-1})[28–32]. Upon irradiation of a solution of **NO_2-OsN** (5×10^{-5} M) in CH_2Cl_2 solution containing excess hydrocarbon (5×10^{-2} M) at 23 °C with blue light-emitting diode (LED) light ($\lambda > 460$ nm), the color of the solution gradually changed from light yellow to brown. The progress of the photochemical reaction was monitored by ultraviolet/visible (UV/Vis) spectrophotometry (vide infra). The rate of the photoreaction decreases with increasing BDE of the substrates, i.e., **XAN**>**DHA**>**EB**»*c*-**OCT**>*c*-**HEX**. No spectral changes were observed in the absence of light. In contrast, **OsN** remains unreactive under similar conditions, in accordance with its much shorter lifetime and lower emission quantum yield in solution.

Silica chromatography of the product solutions afforded two osmium products in each case, an osmium(IV) iminato and an osmium(III) ammine complex, as illustrated in Fig. 5.

Molecular structures. The molecular structure of the osmium (III) ammine complex [PPh_4]**1** was determined by X-ray crystallography (Fig. 2b and Supplementary Table 1). The distorted octahedral arrangement of the parent nitrido complex is retained in the ammine product; the three cyano ligands are in *mer*-configuration. The Os-$N_{(NH3)}$ (Os1-N5) bond length is 2.110(3) Å, typical of a Os-N single bond.

The molecular structures of the osmium(IV) iminato complexes **2, 3, 4** and **5** have also been determined by X-ray crystallography. As shown in Fig. 2c–f, the distorted octahedral arrangement of the ligands around the Os center in the parent **NO_2-OsN** is also retained in these complexes. These complexes all feature a newly formed anionic iminato ligand; the Os-$N_{iminato}$ (Os-N5) bond distances are similar (1.758(11)–1.824(7) Å) and indicative of double bond character. The Os1-N5-C10 bond angles are also similar and close to linear, with an average value of ~174°. The C5-N10 iminato bonds are in a narrow range of 1.246 (12)–1.278(4) Å, typical of a C=N double bond.

1 has a room temperature magnetic moment of $\mu_{eff} = 1.95\,\mu_B$ (Guoy method), consistent with the low-spin d^5 configuration of osmium(III). Complexes **2–5** are diamagnetic, as evidenced by

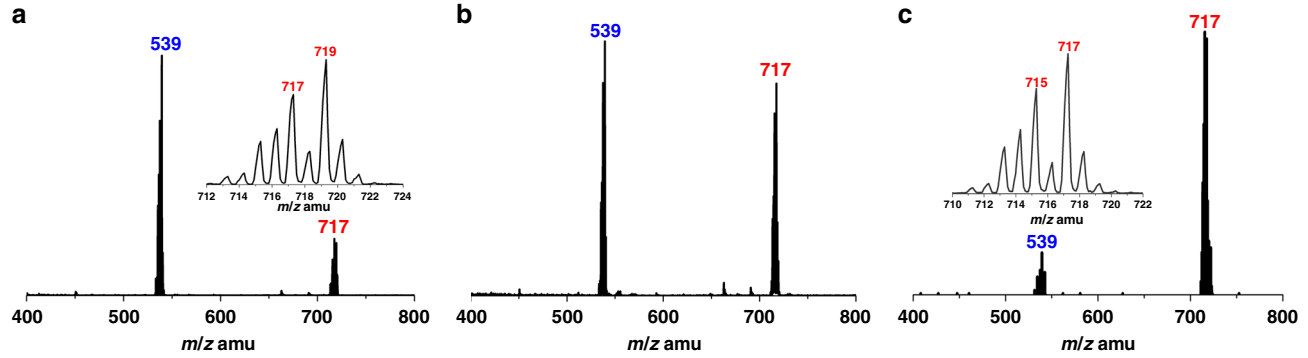

Fig. 6 Electrospray ionization/mass spectrometry (ESI/MS) collected at various irradiation time intervals. **a** **NO_2-OsN** (0.3 mM) and **DHA** (0.3 M) in CH_2Cl_2 is irradiated by visible light for 1 h, **b** for 3 h, and **c** for 12 h. Insets in (**a**, **c**) show the isotopic distribution patterns of the peaks centered at *m/z* 719 and 717

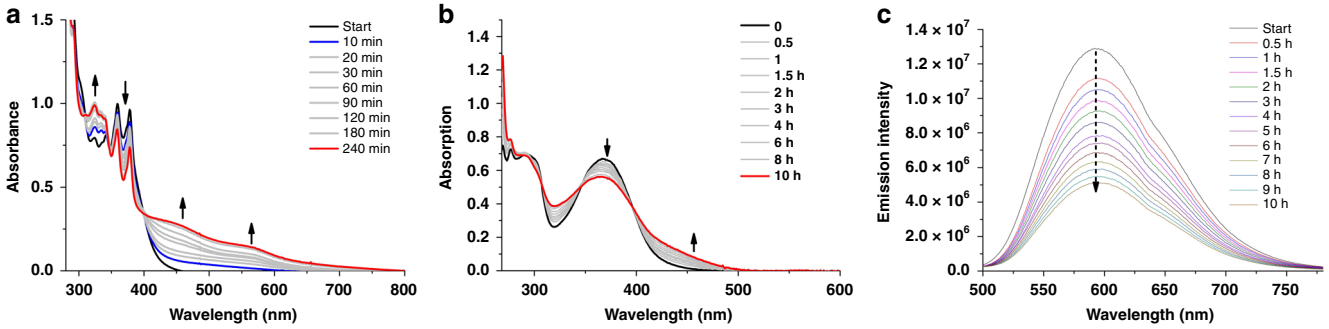

Fig. 7 Spectroscopic traces of **NO_2-OsN** with various substrates. **a** Ultraviolet/visible (UV/Vis) spectral changes for the reaction of **NO_2-OsN** with excess **DHA** in CH_2Cl_2 upon irradiation by blue light-emitting diode (LED). **b** UV/Vis spectral changes for the visible-light irradiation of **NO_2-OsN** and cyclooctane in CH_2Cl_2 under Ar. **c** Emission intensity changes of **NO_2-OsN** and cyclooctane in similar conditions

the sharp resonances in the normal range in the ^{1}H NMR spectrum (Supplementary Figs. 11–12), consistent with the low-spin d^4 electronic configuration of the Os(IV) complexes. **1**–**5** were also characterized by IR spectroscopy, UV/Vis spectroscopy, ESI/MS and electrochemistry (Supplementary Figs. 13–18).

ESI/MS of photochemical reactions. The progress of the photochemical reactions was followed by ESI/MS. The ESI/MS of **NO_2-OsN** in CH_2Cl_2 (−ve mode) shows a predominant parent peak at *m/z* 539. The ESI/MS for the photochemical reaction mixture of **NO_2-OsN** with **DHA** (Fig. 6) shows the appearance of a peak at *m/z* 719, which is assigned to the amido species $[NO_2$-Os-(NH-**DHA**$_{(-H)}$)$]^-$ (see Fig. 9a). This peak is gradually shifted to *m/z* 717, which is consistent with the iminato species **2**, $[NO_2$-Os-(N = **DHA**$_{(-2H)}$)$]^-$. These results suggest that the initially formed amido species undergoes oxidative dehydrogenation to give an iminato complex. After 12 h, the peak at *m/z* 717 becomes predominant, while the peak at *m/z* 539 is further decreased and the isotopic distribution shows that it is a mixture of parent (*m/z* 539) and the ammine complex **1** (*m/z* 542). Similar observations were also found for xanthene, ethylbenzene and cyclooctane (Supplementary Figs. 19–20).

UV/Vis absorption and emission spectroscopy of photochemical reactions. The photochemical reactions of **NO_2-OsN** with excess **XAN, DHA** and **EB** were also monitored by UV/Vis spectroscopy (Fig. 7). In the case of **DHA**, the absorbance at 374 nm due to **NO_2-OsN** decreases with time, while the absorbance from around 410–600 nm increases with time, consistent with the formation of **NO_2-Os=(DHA$_{(-2H)}$)** and **NO_2-OsNH$_3$** with λ_{max} at 444 nm and 459, 551 nm, respectively. Similar UV/Vis spectral changes were observed for the photoreaction of **NO_2-OsN** with **XAN** or **EB** (Supplementary Fig. 21).

The emission spectrum of **NO_2-OsN** is greatly interfered by the emission of the aromatic substrates. On the other hand, the photochemical reaction of **NO_2-OsN** with cyclooctane in CH_2Cl_2 could be followed by both UV/Vis absorption and emission spectroscopy. As shown in Fig. 7b, c, there is a much larger change in emission intensity than in absorbance of the reaction mixture.

Kinetic isotope effects. The kinetic isotope effects (KIE) for the photochemical reaction of **NO_2-OsN** with hydrocarbons were determined by ESI/MS. KIE was found to be ~4.1 from competition experiments using an equimolar mixture of cyclohexane (c-C_6H_{12}) and d^{12}-cyclohexane (c-C_6D_{12}) as substrate (Fig. 8). The KIE was estimated from the ratios of the most intense peaks for the two osmium(IV) iminato products, assuming that the spraying and ionization efficiencies of the two ions are similar. Similarly, the KIE for ethylbenzene was found to be ~7.7 using an equimolar mixture of ethylbenzene ($C_6H_5CH_2CH_3$) and d^{10}-ethylbenzene ($C_6D_5CD_2CD_3$) as substrate. These large KIE values indicate that C–H bond cleavage occurs in the rate-determining step.

Photochemical reaction mechanism. Based on all the experimental results, a mechanism for C–H bond activation by **NO_2-OsN*** is proposed, using **DHA** as an example (Fig. 9a).

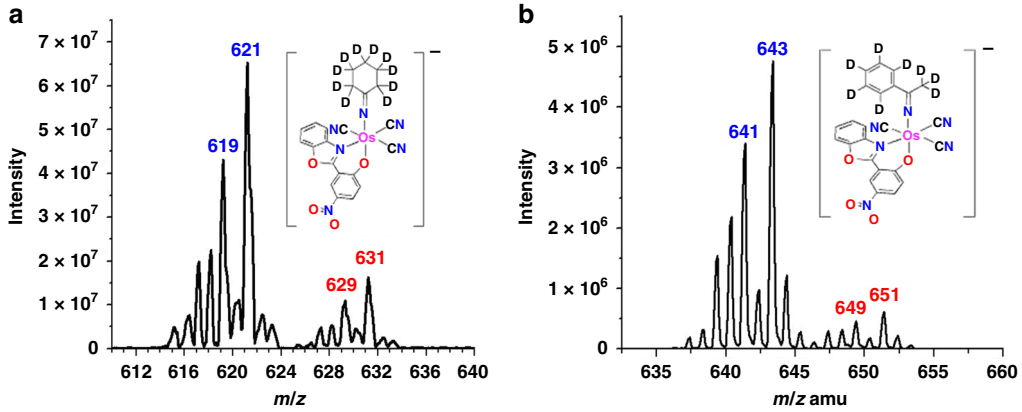

Fig. 8 Kinetic isotope effect (KIE) determination. **a** Electrospray ionization/ mass spectrometry (ESI/MS) showing the KIE effects of cyclohexane. **b** ESI/MS showing the KIE effects of ethylbenzene (red and blue codes are for the product of **NO_2-OsN** with deuterated and normal substrates, respectively)

NO_2-OsN* first abstracts a H-atom from **DHA**; this is followed by a N-rebound process to give an Os^{IV} amido species. These processes are reminiscent of C–H bond activation by metal-oxo species[33–35]. The Os^{IV} amido species undergoes further H-atom abstractions by **NO_2-OsN*** to generate the Os^{IV} iminato product **3**; this is accompanied by the formation of **NO_2-OsNH$_3$** (**1**). For substrates with weak C–H bonds, such as **XAN** and **DHA**, the amido species should be formed more rapidly than its subsequent dehydrogenation, and hence both the amido and the iminato species can be observed by ESI/MS. On the other hand, for ethylbenzene, cyclooctane and cyclohexane, which have stronger C–H bonds, the amido species should be formed much more slowly, hence only the iminato species can be observed.

Photochemical reaction of NO_2-OsN with arenes. **NO_2-OsN*** also readily reacts with anthracene (**ANTH**). ESI/MS of the product solution upon irradiation for 10 h shows two predominant peaks at *m/z* 717 or 731, which are assigned to the osmium(IV) amido species $[Os^{IV}(\mathbf{NO_2\text{-}L})(CN)_3(NH\text{-}\mathbf{ANTH}_{(-H)})]^-$ (**7a**) and the osmium(IV) *p*-benzoquinone iminato species $[Os^{IV}(\mathbf{NO_2\text{-}L})(CN)_3(N{=}\mathbf{ANTH}_{(-2H)}{=}O)]^-$ (**7b**), respectively (Fig. 10).

Both $(PPh_4)[Os^{IV}(\mathbf{NO_2\text{-}L})(CN)_3(NH\text{-}\mathbf{ANTH}_{(-H)})]$ (**[PPh$_4$]7a**) and $(PPh_4)[Os^{IV}(\mathbf{NO_2\text{-}L})(N{=}\mathbf{ANTH}_{(-2H)}{=}O)(CN)_3]$ (**[PPh$_4$]7b**) could be isolated in moderate yields. They are characterized by ^{1}H NMR, IR, ESI/MS, CV and elemental analysis (Supplementary Figs. 22–25).

The molecular structure of $(PPh_4)[Os^{IV}(\mathbf{NO_2\text{-}L})(CN)_3(N{=}\mathbf{ANTH}_{(-2H)}{=}O)]$ ([PPh$_4$]**7b**) has been determined by X-ray crystallography (Fig. 2g). The osmium center is 6-coordinated by three CN^- ligands, a bidentate O^N ligand and a newly formed iminato ligand in a distorted octahedron. The Os-N5 bond length is 1.793(2) Å. The C=N and C=O bond lengths in the newly formed iminato ligand are 1.284(4) and 1.221(4) Å, respectively.

In order to confirm the origin of O atom in resulting complexes, the photochemical reaction of **NO_2-OsN** with anthracene was carried out in the presence of 97% $H_2{}^{18}O$. ESI/MS of the reaction mixture shows that the peak at *m/z* 731 increases by two mass units to *m/z* 733 in the presence of $H_2{}^{18}O$, while the peak at *m/z* 717 remains unchanged (Supplementary Fig. 26). Moreover, no exchange was found between $[Os^{IV}(\mathbf{NO_2\text{-}L})(CN)_3(N{=}\mathbf{Anth}_{(-2H)}{=}{}^{16}O)]^-$ with $H_2{}^{18}O$ in CH_3CN for over 48 h. These results indicate that O atom in **7b** originates from trace H_2O in the reaction system.

In the photochemical reaction of **NO_2-OsN** with anthracene, competition experiments using an equimolar mixture of anthracene and d^{10}-anthracene as substrates were also conducted. A KIE value of around 1.3 (Supplementary Fig. 27) was obtained by ESI/MS; such a small value suggests that the aromatic C–H bond activation does not undergo a HAT/N-rebound process as in aliphatic C–H bond activation. A proposed mechanism is shown in Fig. 9b. **NO_2-OsN*** first undergoes electrophilic attack at the arene to generate immediate I, which then undergoes proton shift to give the amido complex $[Os^{IV}(\mathbf{NO_2\text{-}L})(CN)_3(NH\text{-}\mathbf{ANTH}_{(-H)})]^-$ (**7a**). **7a** then undergoes nucleophilic attack by a water molecule followed by deprotonation to generate intermediate II, which is then oxidized by **NO_2-OsN*** to generate the final *p*-benzoquinone iminato product $[Os^{IV}(\mathbf{NO_2\text{-}L})(CN)_3(N{=}\mathbf{ANTH}_{(-2H)}{=}O)]^-$ (**7b**).

The excited state of **NO_2-OsN** is also able to nitrogenate benzene, although the photoreaction is around 10 times slower than that with anthracene. ESI/MS (−ve mode) of a solution of **NO_2-OsN** and excess benzene (after irradiation for 2 weeks) shows a predominant product peak at *m/z* 631, which is assigned to the species $[Os^{IV}(\mathbf{NO_2\text{-}L})(CN)_3(NC_6H_4O)]^-$ (**8**). In contrast to the anthracene reaction, the intermediate osmium amido species, $[Os^{IV}(\mathbf{NO_2\text{-}L})(CN)_3(NH\text{-}Ph)]^-$, was not observed; presumably the formation of this species is much slower than its subsequent oxidation. The complex $[Os^{IV}(\mathbf{NO_2\text{-}L})(CN)_3(NC_6H_4O]^-$ (**8**) could be isolated as PPh_4^+ salt with about 13% yield. It is characterized by ^{1}H NMR, IR, CV and elemental analysis (Supplementary Figs. 28–29). The X-ray crystal structure of **[PPh$_4$]8** shows Os-N5 bond distance of 1.758(11) Å (Fig. 2h). The C=N and C=O bond lengths in the newly formed ligand are 1.306(18) and 1.231(19) Å, respectively.

Discussion

We have designed a highly luminescent osmium(VI) nitrido complex (**NO_2-OsN**) with long-lived excited state. Experimental results and DFT calculations indicate that the emissive excited state of this complex exhibits LML′CT [π(N^O)→dπ*(Os≡N)] character, which is different from reported luminescent osmium nitrido complexes with predominant *d*–*d* transition character. In accordance with the LML′CT character of its emission, **NO_2-OsN*** possess [Os=N•] nitridyl character, which to our knowledge is the most oxidizing/electrophilic nitrido species reported to date. **NO_2-OsN*** readily undergoes C–H bond activation with alkanes and nitrogenation of arenes, including benzene. In the reaction with alkanes and alkylaromatics, the proposed mechanism involves initial H-atom abstraction from the organic substrate by **NO_2-OsN***, followed by a N-rebound process; which is reminiscent of C–H bond activation by metal-oxo species. On the other hand, reaction with arenes occur by

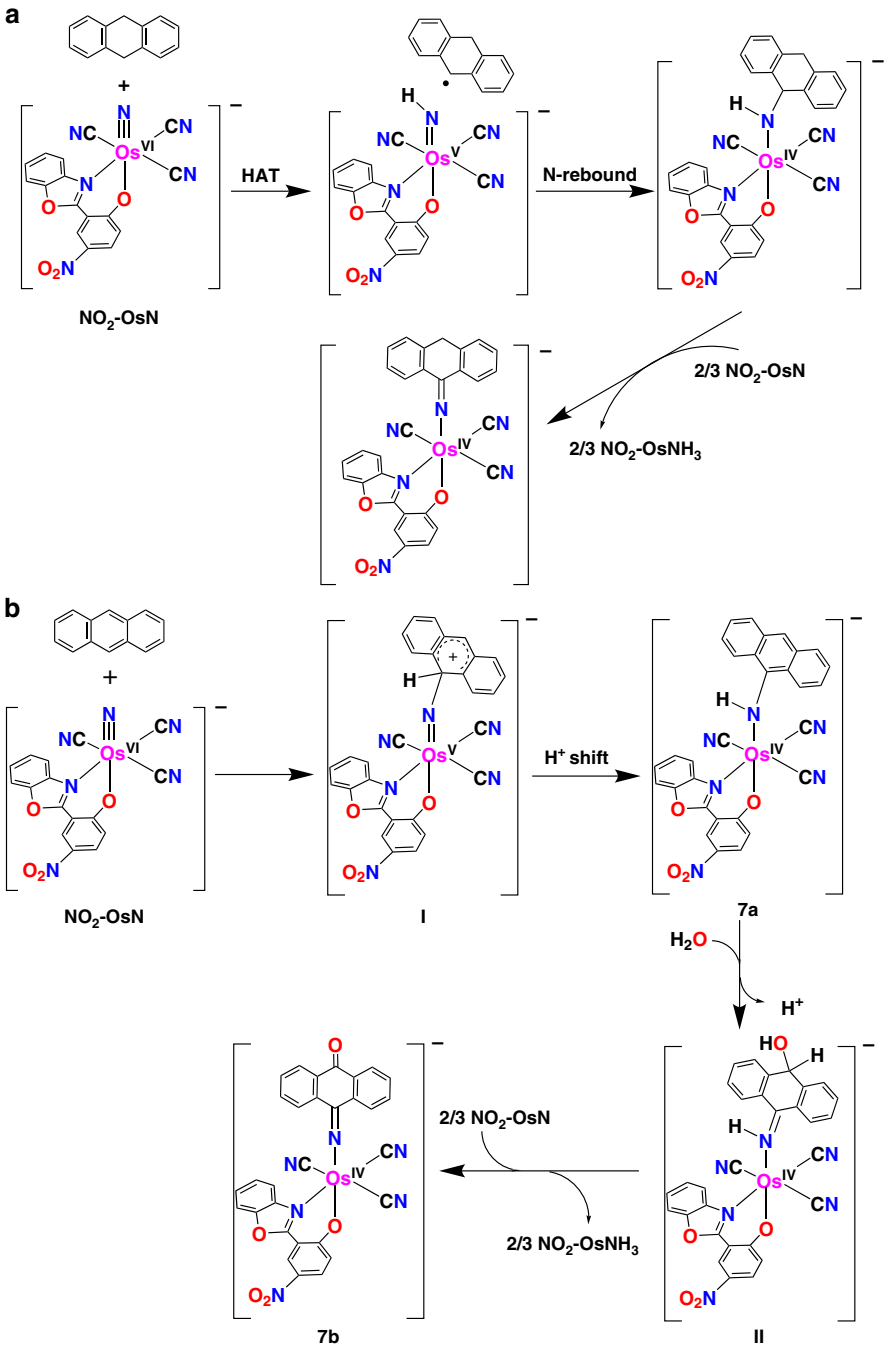

Fig. 9 Proposed reaction mechanisms. **a** The proposed reaction mechanism for **NO_2-OsN*** with **DHA**. **b** The proposed mechanism for the reaction of **NO_2-OsN*** with anthracene

direct electrophilic attack of **NO_2-OsN*** at the aromatic ring. Our results should represent a significant advance in the photochemistry of metal nitrido complexes and in the design of reagents for the nitrogenation of organic substrates using visible light.

Methods

Synthesis of $(PPh_4)[Os^{VI}(N)(NO_2\text{-L})(CN)_3]$ (NO_2-OsN). The procedure is similar to that for **OsN** with minor modifications[22,24]. PhIO (220 mg, 1 mmol) was added to a solution of **NO_2-OsG** (100 mg, 0.1 mmol) in CH_3CN (40 mL), and the mixture was stirred at room temperature for 10 h under Ar. The green solution was evaporated to dryness; the residue was dissolved in a minimum amount of CH_2Cl_2 and then loaded onto a silica gel column. The column was eluted with CH_2Cl_2/acetone (v/v, 10:1) to give a yellow band; the solvent was removed under reduced pressure, and the yellow residue was recrystallized from CH_2Cl_2/Et_2O. Single crystals suitable for X-ray crystallography were obtained by slow diffusion of diethyl ether into a MeCN solution of the compound. Yield: 31 mg, 35%. IR (KBr disc, cm^{-1}): ν(C≡N) 2157 and 2154; ν(N=O) 1322; ν(Os≡N) 1074; ν(Os≡^{15}N) 1046. ^{1}H NMR (400 MHz, $CDCl_3$): δ 8.91 (s, 1H, Ar−H), 7.97−7.90 (m, 6H, Ar−H), 7.80−7.77 (m, 8H, Ar−H), 7.73 (d, J = 8.0Hz, 1H, Ar−H), 7.67−7.62 (m, 8H, Ar−H), 7.55 (d, J = 12.0Hz, 2H, Ar−H), 6.56 (d, J = 9.3Hz, 1H, Ar-H). ESI-MS (−ve mode) in MeOH: m/z 539 (M^-); m/z 540 for ^{15}N-labeled **$NO_2Os^{15}N$**. Anal. Calcd for $C_{40}H_{27}N_6O_4POs$: C, 54.79; H, 3.10; N, 9.58. Found: C, 54.70; H, 3.20; N, 9.60%. UV/Vis (CH_2Cl_2): λ_{max} [nm] (ε [mol^{-1} dm^3 cm^{-1}]): 234sh (63660), 269sh (29270), 276 (33230), 291 (32520), 364 (32400).

Synthesis of $(PPh_4)[Os^{III}(NO_2\text{-L})(CN)_3(NH_3)]$ ($[PPh_4]1$) and $(PPh_4)[Os^{IV}(NO_2\text{-L})(CN)_3(N{=}XAN_{(-2H)})]$ ($[PPh_4]2$). Ten pyrex tubes (15 × 2 cm) each containing **NO_2-OsN** (5 mg, 5.7 μmol) and xanthene (300 mg, 1.6 mmol) in 15 mL

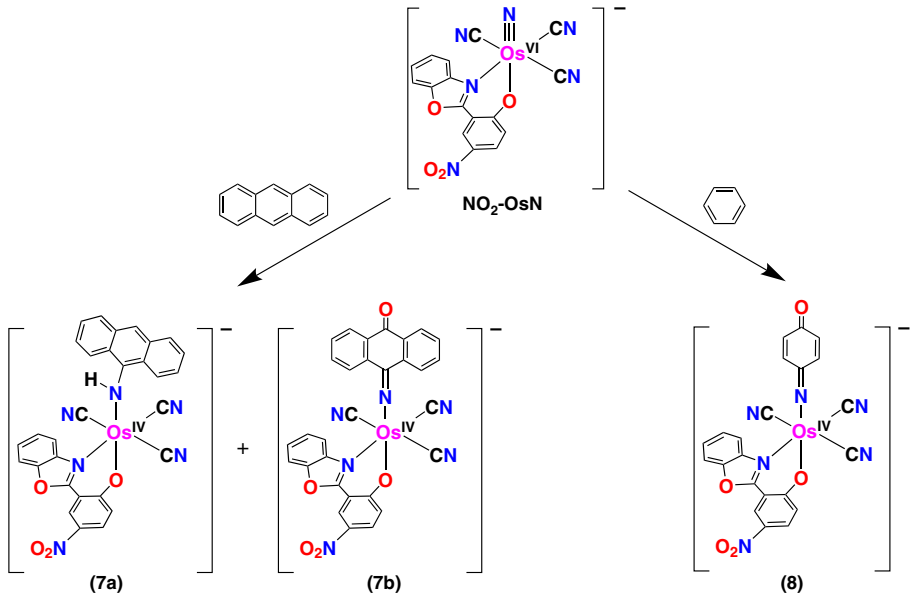

Fig. 10 The reaction pathways of **NO_2-OsN*** with arenes. Photochemical reaction of **NO_2-OsN** with anthracene affords **7a** and **7b**, while its reaction with benzene affords **8**

CH_2Cl_2 were prepared. Each tube was sealed by a rubber septum, degassed with Ar for 30 min and then irradiated with blue LED light for 6 h, whereby the light yellow solution turned red. The solutions were combined and the solvent was removed under reduced pressure. The unreacted xanthene was recovered by extraction with diethyl ether. The solid residue was then dissolved in a minimum amount of CH_2Cl_2 and loaded onto a silica gel column. The first yellow band (unreacted **NO_2-OsN)** was eluted by CH_2Cl_2/acetone (v:v, 10:1). The second green band, which was a mixture of **NO_2-Os-(N = XAN$_{(-2H)}$)** and **NO_2-Os-(NH = XAN$_{(-H)}$)**, was eluted by CH_2Cl_2/acetone (v:v, 4:1). The two complexes were eluted together due to their very similar structures, solubility and polarity. However, **NO_2-Os-**(NH=**XAN**$_{(-H)}$) was slowly oxidized to **NO_2-Os-(N=XAN$_{(-2H)}$)** during the process of recrystallization in air by slow diffusion of diethyl ether into a CH_2Cl_2 solution of the mixture. A third dark red band (**[PPh_4]1)** was eluted by CH_2Cl_2/acetone/MeOH (v:v:v, 20:5:1).

Yield for **[PPh_4]1**: 6 mg, 12%. Selected IR (KBr disc, cm^{-1}): ν(N-H) 3243; ν(C≡N) 2109 and 2086; ν(N=O) 1308. ESI-MS (−ve mode) in MeOH: *m/z* 542 ($[M]^-$), 525 [M - NH_3]$^-$. Anal. Calcd for $C_{40}H_{30}N_6O_4POs$: C, 54.60; H, 3.44; N, 9.55%. Found: C, 54.50; H, 3.50; N, 9.47%. UV/Vis (MeOH): λ_{max} [nm] (ε [mol^{-1} dm^3 cm^{-1}]): 269 (22120), 276 (22200), 294 (20230), 328 (14070), 377 (16600), 411 (11830), 459 (5120), 557 (1710). μ_{eff} = 1.95 μ_B.

Yield for **[PPh_4]2**: 18 mg, 30%. Selected IR (KBr disc, cm^{-1}): ν(C≡N) 2131 and 2122; ν(N=O) 1311; ν(C=N) 1612. ^{1}H NMR (400 MHz, $CDCl_3$): δ 9.04 (s, 1H, Ar-H), 7.96 (d, J = 8.5Hz, 2H, Ar-H), 7.93–7.84 (m, 5H, Ar-H), 7.83–7.74 (m, 9H, Ar-H), 7.72–7.63 (m, 7.9Hz, 8H), 7.60 (d, J = 8.3Hz, 1H, Ar-H), 7.47 (t, J = 7.6Hz, 2H, Ar-H), 7.33 (d, J = 7.9Hz, 3H, Ar-H), 7.02 (dd, J = 15.2, 7.7Hz, 1H, Ar-H), 6.81–6.68 (m, 3H, Ar-H). ESI-MS (−ve mode) in MeOH: *m/z* 719 (M^-). Anal. Calcd for $C_{53}H_{35}N_6O_5POs$: C, 60.22; H, 3.34; N, 7.95. Found: C, 60.30; H, 3.40; N, 7.82%. UV/Vis (CH_2Cl_2): λ_{max} [nm] (ε [mol^{-1} dm^3 cm^{-1}]): 267 (29290), 276 (27830), 287sh (22400), 335 (27740), 384 (24400), 403 (24070), 458 (10880).

Synthesis of (PPh_4)[Os^{IV}(N=DHA$_{(-2H)}$)(NO_2-L)(CN)$_3$] ([PPh_4]3). The procedure is similar to that for **2** except that 9,10-dihydroanthracene (**DHA**) was used instead of xanthene (**XAN**). The reactants in CH_2Cl_2 solution were irradiated with blue light for 24 h and complex **3** was isolated as PPh_4^+ salt by silica gel column chromatography and recrystallization by slow diffusion of diethyl ether into a CH_2Cl_2 solution of **[PPh_4]3**. Yield for **[PPh_4]3**: 19 mg, 32%. Selected IR (KBr disc, cm^{-1}): ν(C≡N) 2136 and 2127; ν(C=N) 1638; ν(N=O) 1313. ^{1}H NMR (400 MHz, $CDCl_3$): δ 9.04 (s, 1H, Ar-H), 8.14 (d, J = 7.5Hz, 2H, Ar-H), 7.98–7.88 (m, 5H, Ar-H), 7.86–7.78 (m, 8H, Ar-H), 7.75–7.66 (m, 8H, Ar-H), 7.67–7.56 (m, 4H, Ar-H), 7.55–7.48 (m, 3H, Ar-H), 6.93 (t, J = 8.3 Hz, 1H), 6.82 (t, J = 8.5 Hz, 3H, Ar-H), 6.37 (s, 2H, -CH_2-). ESI-MS (−ve mode) in MeOH: *m/z* 717 (M^-). Anal. Calcd for $C_{54}H_{37}N_6O_4POs$: C, 61.47; H, 3.53; N, 7.97%. Found: C, 61.40; H, 3.48; N, 8.12%. UV/Vis (CH_2Cl_2): λ_{max} [nm] (ε [mol^{-1} dm^3 cm^{-1}]): 261 (38700), 276 (29850), 285 (23260), 337 (28430), 376sh (22630), 444sh (9660).

Synthesis of (PPh_4)[Os^{IV}(N=EB$_{(-2H)}$)(NO_2-L)(CN)$_3$] ([PPh_4]4). The product was synthesized by a similar procedure as that for **[PPh_4]2** except that ethylbenzene (**EB**) was used instead of xanthene (**XAN**). After irradiation of the reactants in CH_2Cl_2 for 24 h, compound **4** was isolated as PPh_4^+ salt by silica gel column chromatography and recrystallized by slow evaporation of diethyl ether into a CH_2Cl_2 solution of **[PPh_4]4**. Yield for **[PPh_4]4**: 20 mg, 35%. Selected IR (KBr disc, cm^{-1}): ν(C≡N) 2140 and 2126; ν(C=N) 1635; ν(N=O) 1312. ^{1}H NMR (400 MHz, $CDCl_3$): δ 9.00 (s, 1H, Ar-H), 7.95–7.86 (m, 5H, Ar-H), 7.84–7.75 (m, 8H, Ar-H), 7.73–7.63 (m, 9H, Ar-H), 7.59 (d, J = 8.0 Hz, 1H, Ar-H), 7.45 (d, J = 8.3 Hz, 1H, Ar-H), 7.45 (d, J = 8.3 Hz, 1H, Ar-H), 7.24 (s, 1H, Ar-H), 6.97 (dd, J = 17.8, 8.4 Hz, 2H), 6.73 (d, J = 9.1 Hz, 1H, Ar-H), 5.18 (s, 3H, -CH_3). ESI-MS (−ve mode) in MeOH: *m/z* 643 (M^-). Anal. Calcd for $C_{48}H_{35}N_6O_4POs$: C, 58.77; H, 3.60; N, 8.57. Found: C, 58.62; H, 3.50; N, 8.61%. UV/Vis (CH_2Cl_2): λ_{max} [nm] (ε [mol^{-1} dm^3 cm^{-1}]): 261sh (24830), 269 (25790), 276 (23840), 288sh (18510), 329 (26560), 374sh (14480), 433sh (8160).

Synthesis of (PPh_4)[Os^{IV}(NO_2-L)(CN)$_3$(N=*c*-OCT$_{(-2H)}$)] ([PPh_4]5). The product was synthesized using a similar procedure for **[PPh_4]2** except that cyclooctane (***c*-OCT**) was used instead of xanthene (**XAN**). After irradiation for about 72 h, compound **5** was isolated as PPh_4^+ salt by silica gel column purification and further purified from slow evaporation of diethyl ether into a CH_2Cl_2 solution of **[PPh_4]5**. Yield for **[PPh_4]5**: 15 mg, 27%. Selected IR (KBr disc, cm^{-1}): ν(C≡N) 2181 and 2120; ν(C=N) 1630; ν(N=O) 1311; ^{1}H NMR (400 MHz, $CDCl_3$): δ 8.92 (s, 1H, Ar-H), 7.91–7.85 (m, 4H, Ar-H), 7.81 (dt, J = 10.8, 5.4 Hz, 1H, Ar-H), 7.78–7.70 (m, 7H, Ar-H), 7.69–7.63 (m, 2H, Ar-H), 7.64–7.54 (m, 8H, Ar-H), 7.48 (p, J = 7.0 Hz, 2H, Ar-H), 6.81 (d, J = 9.3 Hz, 1H, Ar-H), 4.62 (t, J = 5.7 Hz, 4H, CH_2), 1.73–1.57 (m, 10H). ESI-MS (−ve mode) in MeOH: *m/z* 649 (M^-); Anal. Calcd for $C_{48}H_{41}N_6O_4POs$: C, 58.41; H, 4.19; N, 8.51%. Found: C, 58.32; H, 4.25; N, 8.37%. UV/Vis (CH_2Cl_2): λ_{max} [nm] (ε [mol^{-1} dm^3 cm^{-1}]): 258 (19060), 268 (17640), 276 (16790), 289 (15670), 326 (17520), 370sh (12390), 412sh (9950).

Synthesis of (PPh_4)[Os^{IV}(NO_2-L)(CN)$_3$(NH-ANTH$_{(-H)}$)] ([PPh_4]7a) and (PPh_4)[Os^{IV}(NO_2-L)(CN)$_3$(N=ANTH $_{(-2H)}$ = O)] ([PPh_4]7b). Ten pyrex tubes (15 cm × 2 cm) each containing **NO_2-OsN** (5 mg, 5.7 μmol) and anthracene (**ANTH**, 100 mg, 0.56 mmol) in CH_2Cl_2 (15 mL) were prepared. Each tube was sealed by a rubber septum and degassed with Ar for 30 min. Then, the tubes are irradiated by blue LED light for 2 days, whereby the light yellow solutions turned brown. The solutions in the tubes were combined and the solvent was removed under reduced pressure. The residue was washed with diethyl ether (100 mL) to remove the unreacted anthracene. The solid was then dissolved in a minimum amount of CH_2Cl_2 and then loaded onto a silica gel column. The first light yellow band, (PPh_4)[Os^{IV}(**NO_2-L**)(N=**ANTH** $_{(-2H)}$=O)(CN)$_3$] (**[PPh_4]7b**), was eluted by CH_2Cl_2/Acetone (9:1) and the second band (PPh_4)[Os^{IV}(**NO_2-L**)(NH-**ANTH**$_{(-H)}$)(CN)$_3$] (**[PPh_4]7a**) was eluted by CH_2Cl_2/Acetone (4:1).

Yield for **[PPh_4]7a**: (7 mg, 12%). Selected IR (KBr disc, cm^{-1}): ν(N-H) 3248; ν(C≡N) 2145 and 2128; ν(N=O) 1314. ^{1}H NMR (400 MHz,$CDCl_3$): δ 9.00 (d, J = 2.8 Hz, 1H); 8.13 (d, J = 7.8 Hz, 2H); 7.97–7.84 (m, 6H); 7.83–7.74 (m, 8H); 7.69–7.63 (m, 8H); 7.62–7.52 (m, 3H); 7.49 (d, J = 7.7 Hz, 1H); 7.29 (dd, J = 13.0, 5.2 Hz, 2H); 6.90 (t, J = 7.8 Hz, 1H); 6.84–6.74 (m, 3H); ESI-MS (−ve mode) in MeOH: *m/z* 717 (M^-); Anal. Calcd for $C_{54}H_{37}N_6O_4OsP$: C, 61.47; H, 3.53; N, 7.97. Found: C, 61.40; H,

3.62; N, 7.90%. UV/Vis (CH_2Cl_2): λ_{max} [nm] (ε [mol^{-1} dm^3 cm^{-1}]): 232 (91670), 261 (59390), 276sh (47080), 337 (44270), 374sh (35790), 447sh (15430).

Yield for **[PPh_4]7b**: (9 mg, 15%). Selected IR (KBr disc, cm^{-1}): ν(C≡N) 2149 and 2129; ν(C=O) 1704 and 1649; ν(C=N) 1612 and 1596; ν(N=O) 1312. ^{1}H NMR (400 MHz,$CDCl_3$): δ 9.03 (d, J = 2.9 Hz, 1H); 8.59–8.53 (m, 2H); 8.37 (d, J = 8.0 Hz, 2H); 8.04 (dd, J = 9.4, 2.9 Hz, 1H); 7.98–7.92 (m, 2H); 7.90–7.84 (m, 4H); 7.76 (td, J = 7.8, 3.6 Hz, 9H); 7.67–7.56 (m, 9H); 7.52 (d, J = 8.2 Hz, 1H); 7.33 (t, J = 7.9 Hz, 1H); 7.02–6.89 (m, 4H). ESI-MS (−ve mode) in MeOH: m/z 731 (M^-); Anal. Calcd for $C_{54}H_{35}N_6O_5OsP$: C, 60.67; H, 3.30; N, 7.86. Found: C, 60.55; H, 3.35; N, 7.79%. UV/Vis (CH_2Cl_2): λ_{max} [nm] (ε [mol^{-1} dm^3 cm^{-1}]): 236 (74870), 244 (65420), 270 (34320), 277 (35700), 286 (31110), 336 (29430), 439 (30840)

Synthesis of (PPh_4)[$Os^{IV}(NO_2\text{-}L)(CN)_3(N{=}Ph{=}O_{(-2H)})$] ([$PPh_4$]8). The synthetic route for **[PPh_4]8** is similar to that of **[PPh_4]7a** except that benzene (2 mL) was used instead of anthracene, and the duration of the irradiation was 2 weeks. Yield for **[PPh_4]8**: (7.7 mg, 14%). Selected IR (KBr disc, cm^{-1}): ν(C≡N) 2149 and 2140; ν(C=O) 1623; ν(C=N) 1615; ν(N=O) 1307. ^{1}H NMR (400 MHz, $CDCl_3$): δ 9.08 (d, J = 2.8 Hz, 1H); 8.40 (d, J = 9.8 Hz, 2H); 8.20–8.13 (m, 1H); 7.98–7.90 (m, 4H); 7.86–7.72 (m, 10H); 7.71–7.56 (m, 10H); 7.07 (d, J = 9.3 Hz, 1H); 6.92 (t, J = 7.4 Hz, 2H). ESI-MS (−ve mode) in MeOH: m/z 631 (M^-); Anal. Calcd for $C_{46}H_{31}N_6O_5POs$: C, 57.02; H, 3.22; N, 8.67. Found: C, 57.10; H, 3.17; N, 8.70%. UV/Vis (CH_2Cl_2): λ_{max} [nm] (ε [mol^{-1} dm^3 cm^{-1}]): 233 (76260), 239 (60300), 270 (39090), 277 (41510), 295 (38530), 337 (36260), 349 (35200), 427 (42520), 450 (34000).

Data availability

We declare that the data supporting the findings of this study are available within the article and Supplementary Information file or from the corresponding author upon reasonable request. The X-ray crystallographic coordinates for structures reported in this Article have been deposited at the Cambridge Crystallographic Data Centre (CCDC), under deposition number CCDC 1871861–1871868. These data can be obtained free of charge from The Cambridge Crystallographic Data Centre via http://www.ccdc.cam.ac.uk/data_request/cif.

Received: 19 November 2018 Accepted: 4 March 2019
Published online: 29 March 2019

References

1. Eikey, R. A. & Abu-Omar, M. M. Nitrido and imido complexes of groups 6-8. *Coord. Chem. Rev.* **243**, 83–124 (2003).
2. Berry, J. F. Terminal nitrido and imido complexes of late transition metals. *Comments Inorg. Chem.* **30**, 28–66 (2009).
3. Smith, J. M. Reactive transition metal nitride complexes. *Progress Inorg. Chem.* **58**, 417–470 (2014).
4. Meunier, B., de Visser, S. P. & Shaik, S. Mechanism of oxidation reactions catalyzed by cytochrome P450 enzymes. *Chem. Rev.* **104**, 3947–3980 (2004).
5. Ortiz de Montellano, P. R. *Cytochrome P450. Structure, Mechanism and Biochemistry* (Plenum, New York, 1995).
6. Meyer, T. J. & Huynh, M. H. V. The remarkable reactivity of high oxidation state ruthenium and osmium polypyridyl complexes. *Inorg. Chem.* **42**, 8140–8160 (2003).
7. Man, W. L., Lam, W. W. Y. & Lau, T. C. Reactivity of nitrido complexes of ruthenium(VI), osmium(VI), and manganese(V) bearing Schiff base and simple anionic ligands. *ACC Chem. Res.* **47**, 427–439 (2014).
8. Man, W. L., Lam, W. W. Y., Kwong, H. K., Yiu, S. M. & Lau, T. C. Ligand-accelerated activation of strong C-H bonds of alkanes by a (Salen) ruthenium(VI)–nitrido complex. *Angew. Chem. Int. Ed.* **51**, 9101–9104 (2012).
9. Long, A. K. M., Yu, R. P., Timmer, G. H. & Berry, J. F. Aryl C−H bond amination by an electrophilic diruthenium nitride. *J. Am. Chem. Soc.* **132**, 12228–12230 (2010).
10. Long, A. K. M. et al. Aryl C–H amination by diruthenium nitrides in the solid state and in solution at room temperature: experimental and computational study of the reaction mechanism. *J. Am. Chem. Soc.* **133**, 13138–13150 (2011).
11. Atienza, C. C. H., Bowman, A. C., Lobkovsky, E. & Chirik, P. J. Photolysis and thermolysis of Bis(imino)pyridine cobalt azides: C−H activation from putative cobalt nitrido complexes. *J. Am. Chem. Soc.* **132**, 16343–16345 (2010).
12. Cui, P. et al. Ring-size-modulated reactivity of putative dicobalt-bridging nitrides: C-H activation versus phosphinimide formation. *Angew. Chem. Int. Ed.* **56**, 15979–15983 (2017).
13. Hennig, H., Hofbauer, K., Handke, K. & Stich, R. Unusual reaction pathways in the photolysis of diazido(phosphane)nickel(ii) complexes: nitrenes as intermediates in the formation of nickel(0) complexes. *Angew. Chem. Int. Ed. Engl.* **36**, 408–410 (1997).
14. Thomson, R. K. et al. Uranium azide photolysis results in C–H bond activation and provides evidence for a terminal uranium nitride. *Nat. Chem.* **2**, 723–729 (2010).
15. Che, C.-M., Lam, M. H.-W. & Mak, T. C. W. Metal nitrido and imido photo-oxidants. Photophysics and photochemistry of nitrido and imido complexes of osmium(VI) and X-ray crystal structure of $[Ph_4As]_2[Os^{VI}(CN)_5N]$.*J. Chem. Soc. Chem. Commun.* **20**, 1529–1531 (1989).
16. Chin, K. F., Cheung, K. K., Yip, H. K., Mak, T. C. W. & Che, C. M. Luminescent nitridometal complexes, photophysical and photochemical properties of the $^3[(d_{xy})^1(d_{\pi^*})^1]$ excited state of nitridoosmium(VI) complexes with polypyridine ligands. *J. Chem. Soc. Dalton Trans.* 657–663 (1995).
17. Hopkins, M. D., Miskowski, V. M. & Gray, H. B. Luminescence from nitrido complexes of osmium(VI). Evidence for a nontotally symmetric excited-state distortion. *J. Am. Chem. Soc.* **108**, 6908–6911 (1986).
18. Che, C. M., Lau, T. C., Lam, H. W. & Poon, C. K. Metal-nitrido photo-oxidants: synthesis, photophysics and photochemistry of $[Os^{VI}(NH_3)_4(N)](X)_3$ (X=Cl, CF_3SO_3). *J. Chem. Soc., Chem. Commun.* 114–116 (1986).
19. Lai, S. W., Lau, T. C., Fung, W. K. M., Zhu, N. Y. & Che, C. M. Luminescent nitridoosmium(VI) complexes with aryl- and alkylacetylide ligands: spectroscopic properties and crystal structures. *Organometallics* **22**, 315–320 (2003).
20. Ikeda, H. et al. Photoluminescence switching with changes in the coordination number and coordinating volatile organic compounds in tetracyanidonitridorhenium(V) and -technetium(V) complexes. *Inorg. Chem.* **51**, 12065–12074 (2012).
21. Ikeda, H. et al. Excited-state characteristics of tetracyanidonitridorhenium(V) and -technetium(V) complexes with N-heteroaromatic ligands. *Inorg. Chem.* **52**, 6319–6327 (2013).
22. Xiang, J., Man, W. L., Yiu, S. M., Peng, S. M. & Lau, T. C. Reaction of an osmium(VI) nitrido complex with cyanide: formation and reactivity of an osmium(III) hydrogen cyanamide complex. *Chem. Eur. J.* **17**, 13044–13051 (2011).
23. Xiang, J. et al. Aerobic oxidation of an osmium(III) *N*-hydroxyguanidine complex to give nitric oxide. *Inorg. Chem.* **55**, 5056–5061 (2016).
24. Xiang, J., Wang, Q., Yiu, S. M. & Lau, T. C. Dual pathways in the oxidation of an osmium(III) guanidine complex. formation of osmium(VI) nitrido and osmium nitrosyl complex. *Inorg. Chem.* **56**, 2022–2028 (2017).
25. Wong, T. W., Lau, T. C. & Wong, T. W. Osmium(VI) nitrido and osmium (IV) phosphoraniminato complexes containing Schiff base ligands. *Inorg. Chem.* **38**, 6181–6186 (1999).
26. Scepaniak, J. J. et al. Structural and spectroscopic characterization of an electrophilic iron nitrido complex. *J. Am. Chem. Soc.* **130**, 10515–10517 (2008).
27. Scheibel, M. G. et al. Closed-shell and open-shell square-planar iridium nitrido complexes. *Nat. Chem.* **4**, 552–558 (2012).
28. Mayer, J. M. Understanding hydrogen atom transfer: from bond strengths to Marcus theory. *ACC Chem. Res.* **44**, 36–46 (2011).
29. Bordwell, F. G., Cheng, J. P., Ji, G. Z., Satish, A. V. & Zhang, X. Bond dissociation energies in DMSO related to the gas phase values. *J. Am. Chem. Soc.* **113**, 9790–9795 (1991).
30. Lide, D. R. (ed.) *CRC Handbook of Chemistry and Physics*, 82nd edn (CRC Press, Boca Raton, 2001).
31. Borovik, A. S. Role of metal–oxo complexes in the cleavage of C–H bonds. *Chem. Soc. Rev.* **40**, 1870–1874 (2011).
32. Luo, Y. R. *Handbook of Bond Dissociation Energies in Organic Compounds* (CRC Press, Boca Raton, 2003).
33. Gunay, A. & Theopold, K. H. C−H bond activations by metal oxo compounds. *Chem. Rev.* **110**, 1060–1081 (2010).
34. Nam, W. High-valent iron(IV)–oxo complexes of heme and non-heme ligands in oxygenation reactions. *ACC Chem. Res.* **40**, 522–531 (2007).
35. McLain, J. L., Lee, J. & Groves, J. T. in *Biomimetic Oxidations Catalyzed by Transition Metal Complexes* (ed. Meunier, B) 91–170 (Imperial College, London, 2000).

Acknowledgements

This work was supported by the National Natural Science Foundation of China (21771026), Hubei Provincial Natural Science Foundation of China (2018CFA047), the Research Grants Council of Hong Kong (CityU 11302917) and the Hong Kong University Grants Committee (AoE/P-03–08).

Author contributions

J.X. designed and carried out the experiments. X.-X.J., Q.-Q.S. and W.-L.M. solved the X-Ray structures. S.-C.C. and C.-C.K investigated the photophysical properties. M.X. and L.W. performed computational studies. C.-M.C. and T.-C.L. designed the study. J.X. and

T.-C.L. analyzed the data and wrote the paper. All authors discussed the results and commented on the manuscript.

Additional information

Supplementary information accompanies this paper at https://doi.org/10.1038/s42004-019-0142-3.

Competing interests: The authors declare no competing interests.

Reprints and permission information is available online at http://npg.nature.com/reprintsandpermissions/

Publisher's note: Springer Nature remains neutral with regard to jurisdictional claims in published maps and institutional affiliations.